Effects of composition on transformation temperatures and microstructure of Ni-Ti-Hf shape memory alloys

http://dx.doi.org/10.1590/0370-44672018720072

Roniere Leite Soares[1,3]
https://orcid.org/0000-0003-2784-4468
Walman Benício de Castro[2,4]
https://orcid.org/0000-0002-4338-9488

[1]Universidade Federal de Campina Grande – UFCG, Unidade Acadêmica em Engenharia de Produção – UAEP, Programa de Pós-Graduação em Ciência e Engenharia de Materiais – PPGCEMat, Campina Grande – Paraíba – Brasil.

[2]Universidade Federal de Campina Grande – UFCG, Unidade Acadêmica de Engenharia Mecânica – UAEMec, Programa de Pós-Graduação em Ciência e Engenharia de Materiais – PPGCEMat, Campina Grande – Paraíba – Brasil.

E-mails: [3]ronieter@gmail.com, [4]walman_benicio@hotmail.com

Abstract

High transformation temperature shape-memory alloys (HTSMA) usually present a martensitic transformation temperature (Ms) starting at 100 ºC. That is the case of high nickel Ni-Ti-Hf alloys. This article presents experimental results obtained from arc melting of $Ni_{50}Ti_{50-X}Hf_X$ .at% (X = 8, 11, 14, 17 and 20 .at%) alloys. This process homogenized every composition with similar relative crystallinity. Results confirm that transformation temperatures (TT) increase with increasing the amount of Hf. A martensitic matrix is formed by two metastable phases: R and B19'. From all the alloys studied, the B19' phase presented the highest percent fraction. Gradually adding Hf_3 .at% promoted a slow increase of crystalline fraction of R phase and a slow reduction of phase $(Ti, Hf)_2$ Ni, located at grain boundaries. Coherent/semi-coherent interface between $(Ti, Hf)_2$ Ni phase and the matrix may intensify the driving force for the formation of R phase, present on X-ray diffractograms.

Keywords: high temperature shape memory alloys; Ni-Ti-Hf alloys; microstructure.

1. Introduction

SMA are materials that have the ability to retrieve their original shape under appropriate thermal conditions. This is possible due to a solid state phase transformation named Thermoelastic Martensitic Transformation which restores great deformations (between 8 and 10%) (Besseghini *et al*., 1999).

Some SMA from the NiTi system are considered HTSMA (high temperature shape memory alloys) (Humbeeck, 2012). To these alloys is added a third element (Ni-Ti-X) which, depending on the process and the amount added, may result in martensitic transformation temperatures starting above 100 ºC (Ma *et al*., 2010; Karaca *et al*., 2013). Examples of these alloys are: Ti-Ni-Pd (Kockar *et al*., 2010), Ti-Ni-Pt (Kovarik *et al*., 2010), Ti-Ni-Ta (Gong *et al*., 2006), Ti-Ni-Au (Shi *et al*., 2014) and Ni-Ti-Hf (Manca *et al*., 2003).

Among these tertiary elements that favor high temperature applications of SMA, Hf is a chemical element economically accessible. There are three kinds of Ni-Ti-Hf SMA: interstitial ($Ni_{50-X}Ti_{50}Hf_X$ .at%: rich in titanium), equiatomic ($Ni_{100-X/2}Ti_{100-X/2}Hf_X$ .at% ($5 \leq X \leq 20$)) and substitutional ($Ni_{50}Ti_{50-X}Hf_X$ .at%: rich in nickel) (Zarinejad *et al*., 2008). The present paper studied the latter due to the fact that it has been broadly discussed in literature (Sanjabi *et al*., 2005), when compared to the former two kinds. The objective of this study was to perform a thermal, physical and structural characterization of $Ni_{50}Ti_{50-X}Hf_X$ .at% shape memory alloys, adding Hf as a substitutional atom to Ti. This study contributes to practical applications of advanced materials such as sensors and actuators in the most varied sectors: automotive, oil and aerospace (Karaca *et al*., 2013).

The major difference of this article is the level of detail given to the crystalline fractions and their respective constituent phases, correlating them with the contents of added Hf and heat treatments, besides approaching them qualitatively and quantitatively based on nominal compositions not yet examined by literature.

2. Experimental procedure

Five nominal compositions of $Ni_{50}Ti_{50-X}Hf_X$ .at% alloy were prepared with pure Ni (99.98%), Ti (99.99%) and Hf (99.95%) in an arc melt furnace, as shown in Figure 1(d). The elements were placed accordantly to its melting temperature, in a way that elements with higher melting point stayed on top of the others, as presented in Figure 1(a). This procedure ensures that all elements will melt. The preparation of the metal portions was done by using a method that starts with the calculation of the Proportional Masses of the "n" chemical elements involved in the nominal composition (Soares, 2016), as explained in Table 1.

Table 1
Methodology used to prepare 10 grams of $Ni_{50}Ti_{42}Hf_8$ .at% alloy.

Method	Elements →	Ni	Ti	Hf	[Σ]
Nominal Atomic Percentage	%.atn	50	42	8	100
Molar Mass	K	58.69	47.86	178.49	---
Proportional Mass	Mpn	2934.5	2010.12	1427.92	6372.54
Proportional Quantity of Atoms	$QtyPROP_{atoms}$	3.01107×10^{25}	2.5293×10^{25}	4.81771×10^{24}	6.02214×10^{25}
Mass Percentage	%.wtn (1/100)	0.460491421	0.315434662	0.224073917	1
Mass Percentage (rounded)	%.wtn	46.05	31.54	22.41	100
Partial real masses [g]	Mrp	4.604	3.155	2.24	Mr_{total} = 10 g
Real Amount of Atoms	$QtyREAL_{atoms(n)}$	4.72413×10^{22}	3.96988×10^{22}	7.55762×10^{21}	9.44978×10^{22}

The elements used were previously weighed (analytical scale with a precision of 0.0001g) considering 10 g of alloy and pickled (chemical process of superficial oxidation removal) with acid solutions. Next, the samples were cleaned with acetone or ethylic alcohol under ultrasonic agitation. The elements were then melted to a single ingot and remelted three times taking care to flip the ingot over between each melt in order to achieve a higher composition homogeneity.

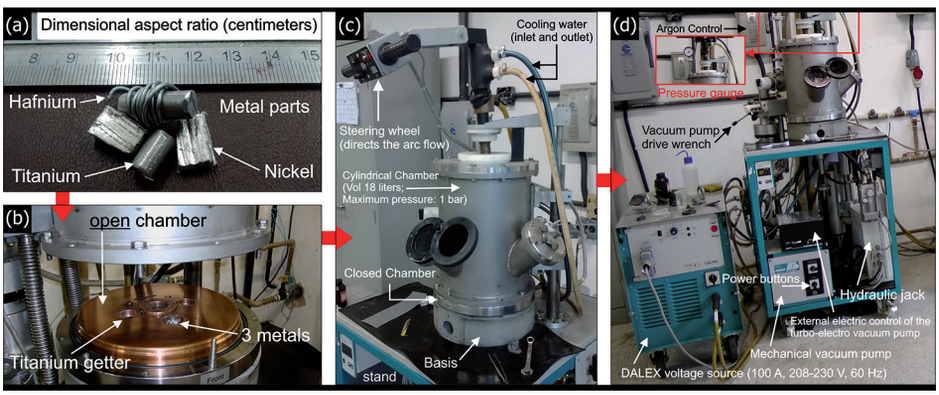

Figure 1
(a) chemical elements Ni, Ti and Hf; (b) open chamber of the arc melting furnace and arrangement of metals in bas-relief; (c) bench with closed chamber for evacuation, purge and melting; (d) external elements of the furnace and gauge detail.

The chamber of arc melting shown in Figure 1(c) was evacuated to 10^{-5} Torr and filled with ultrapure argon at 0.5 atm; this purge process was repeated three times. At the last purge, the chamber was pressurized with argon at 0.9 atm. The residual oxygen was eliminated by melting and cooling a titanium getter (figure 1(b)) for at least two times. This is extremely important because the slightest change in composition and the presence of a few ppm of oxygen may change the properties of the alloy. The maximum torch temperature in the furnace is about 3600 °C and time of incidence on the metals was around 15 seconds (each melting).

Thermal characterization of the alloys was performed by differential scanning calorimetry (DSC) using equipment 404 from Netzsch with a heating rate of 10 °C/min in a copper crucible in an ultrapure argon (99.998%) atmosphere.

An X-ray Diffraction (XRD) technique was used to identify phases and compounds in the alloys aided by X'Pert HighScore Plus V3.0 software from PANanalytical. The equipment employed was a SHIMADZU X-ray diffractometer model XRD 6000, operating with CuKα radiation (λ = 1.54056 Å), at a voltage of 40 kV and current of 30 mA. The 2θ scan (12°- 90 °) was from 78 ° and speed of 2 °/min. Slits used were:: (i) divergence = 1 °; (ii) dispersion = 1°; e (iii) reception = Ø 0.3 mm. Data collected were enough for structure refinement by the least-squares method (Rietveld, 1967). It was also possible to perform the indexation of crystallographic planes. Results obtained presented chi-squared $X^2 = (R_{wp}/R_{exp})^2$ or GOF (goodness of fit) lower than three ($X^2 < 3$), which is a value considered acceptable by the international crystallographic union.

The relative degree of crystallinity $X_c = I_{calc}/(_{Icalc} + I_{back}).100$ was calculated considering the sum of integrated areas, of peaks (calculated intensities) and of base line (background intensitie) (Colman *et al.*, 2014). Icalc were adjusted by the Pseudo-Voigt function (gaussian + lorentzian) and Iback was modeled by Sonnevelds's empiric polinomy (Sonneveld e Visser, 1975), composed by two coefficients.

For microstructural characterization and determination of chemical composition, samples were ground, polished and etched with a solution of H_2O:HNO_3:HF and then observed by a Scanning Electron Microscope (SEM), model VEGA 3 from TESCAN, with EDS module, which does not have a heating/cooling chamber.

3. Results and discussion

Figure 2 presents normalized room temperature diffractograms of the alloys studied. Diffracted peaks revel the presence of Ni-Ti-Hf matrix formed by B19' (monoclinic structure) and R (rhombohedral) phases, in addition to the $(Ti, Hf)_2$ Ni (cubic) precipitated phase.

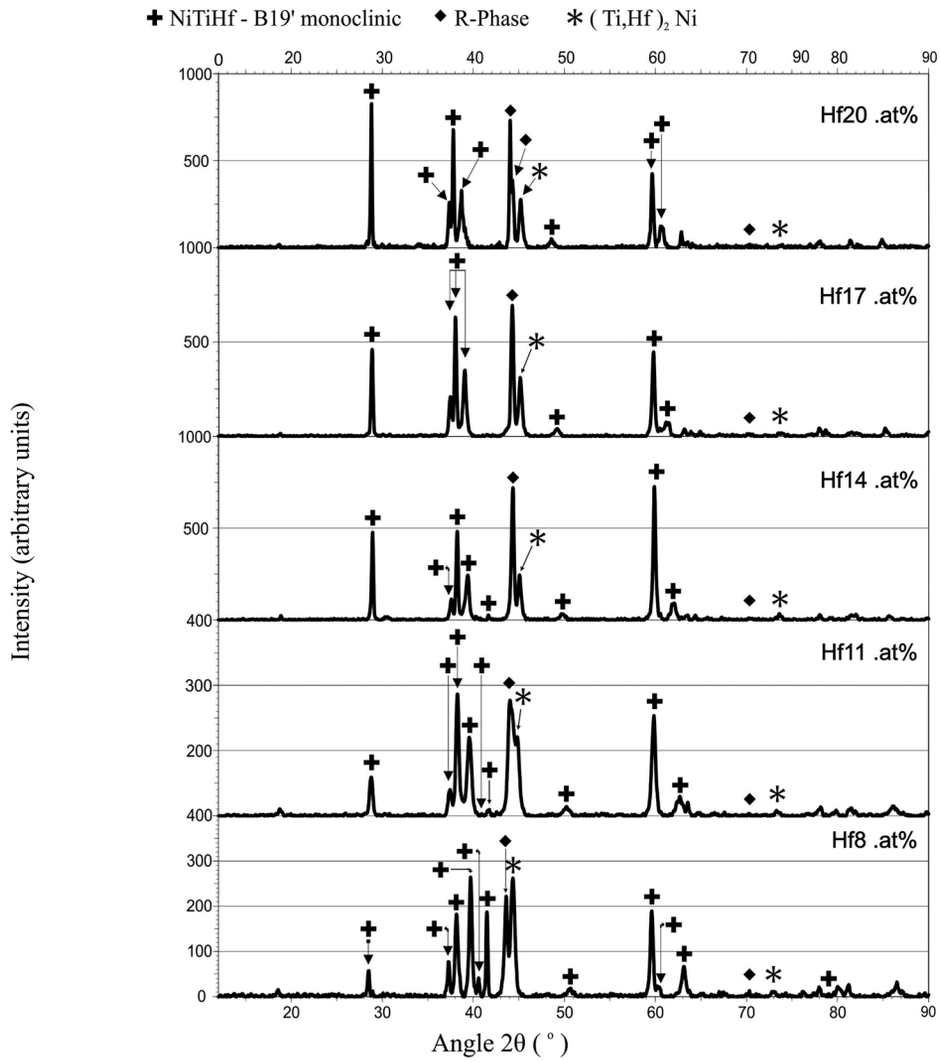

Figure 2
CuKα1 radiation diffractograms of the five $Ni_{50}Ti_{50-X}Hf_X$ at.% alloys.

B19' phase is predominant throughout the entire martensitic matrix. Lattice parameters of the monoclinic structure ($a \neq b \neq c$; $\alpha = \gamma = 90°$ and $\beta \neq 90°$) were obtained by Rietveld refinement (Rietveld, 1969). Results are presented in Table 2 and show that the volume of the crystalline cell (space group P 1 21/m 1) evolves as the content of Hf increases.

Unit Cell	Hf8 .at%	Hf11 .at%	Hf14 .at%	Hf17 .at%	Hf20 .at%
a [Å]	2.97665	3.00172	3.01369	3.15053	3.54281
b [Å]	4.12345	4.10586	4.09231	4.02321	4.00745
c [Å]	4.75868	4.76631	4.80082	4.93231	5.11067
β [°]	99.35657	99.54996	101.2781	105.79572	112.0121
Volume [Å³]	57.63131	57.929	58.06492	60.15744	67.27032
Crystallite Size [Mean, µm]	0.02	0.03	0.01	0.05	0.02
GOF (X^2)	2.00	1.69	1.09	1.96	2.47

Table 2
Unity cells parameters of $Ni_{50}Ti_{50-X}Hf_X$ .at% alloys.

The characterization of B19'phase, refined using Card 99-003-0004, allowed the calculation of Miller indexes (h k l), as shown in Table 3. The number of indexed peaks with only the B19'phase was 77 (at the Hf8 .at% alloy), 73 (at the Hf11 .at% alloy), 20 (at the Hf14 .at% alloy), 233 (at the Hf17 .at% alloy) and 194 (at the Hf20 .at% alloy). As an example, the nominal composition $Ni_{50}Ti_{36}Hf_{14}$ .at% alloy was chosen to show the indexation of crystalline planes in Table 3. The adjustment of the values obtained reveals that there was a great fitting of experimental data in relation to standard CIF values, besides demonstrating a good level of repetition of this structure in the crystalline reticulate.

The characterization of B19'phase, refined using Card 99-003-0004, allowed the calculation of Miller indexes (h k l), as shown in Table 3. The number of indexed peaks with only the B19'phase was 77 (at the Hf8 .at% alloy), 73 (at the Hf11 .at% alloy), 20 (at the Hf14 .at% alloy), 233 (at the Hf17 .at% alloy) and 194 (at the Hf20 .at% alloy). As an example, the nominal composition $Ni_{50}Ti_{36}Hf_{14}$ .at% alloy was chosen to show the indexation of crystalline planes in Table 3. The adjustment of the values obtained reveals that there was a great fitting of experimental data in relation to standard CIF values, besides demonstrating a good level of repetition of this structure in the crystalline reticulate.

2θ	FWHM	Indexes			Area	d-spacing	Height	Rel. Int.	Integral Breadth
[°]	[°2θ]	h	k	l	[cts*°2θ]	[Å]	[cts]	[%]	[°2θ]
18.87	0.1442	0	0	1	3.53	4.69938	23.72	3.13	0.148749
28.93	0.2047	0	1	1	140.39	3.08386	526.82	69.52	0.266489
30.50	0.6554	1	0	0	15.52	2.92831	17.77	2.34	0.87338
37.58	0.2923	1	1	0	57.22	2.39177	117.66	15.53	0.486335
38.23	0.2401	0	0	2	162.64	2.35241	515.05	67.97	0.315776
39.35	0.4647	1	1	-1	186.14	2.28775	256.68	33.87	0.725185
44.33	0.3063	0	1	2	337.81	2.04167	757.78	100	0.445784
45.11	0.388	1	1	1	115.64	2.00826	226.3	29.86	0.510999
49.79	0.7931	1	1	-2	27.44	1.8298	31.21	4.12	0.879182
59.89	0.3125	0	2	2	338.74	1.54313	755.79	99.74	0.448191
61.99	0.7052	2	0	-1	100.42	1.49592	105.41	13.91	0.952691
63.36	0.8196	0	1	-3	34.16	1.4668	31.44	4.15	1.086674
64.38	0.3846	1	2	-2	10.69	1.44599	26.04	3.44	0.410604
65.65	0.7134	1	1	-3	11.28	1.42101	10.5	1.39	1.074187
70.27	0.1112	2	0	1	3.72	1.33855	16.25	2.14	0.229179
73.64	0.5942	1	0	3	14.75	1.28529	24.07	3.18	0.612757
78.05	0.3785	1	3	-1	20.48	1.2233	31.05	4.1	0.659502
79.28	0.6652	2	2	-1	17.98	1.20741	14.89	1.97	1.207022
81.79	0.9219	0	0	4	24.72	1.17661	26.01	3.43	0.950725
85.82	1.3669	0	1	4	49,44	1.13135	17.55	2.32	2.817182

Table 3
Indexation of 20 peaks of B19' phase in $Ni_{50}Ti_{36}Hf_{14}$ .at% alloy.

The calculated relative crystallinity was 58.16% (Hf8 .at%), 63.88% (Hf11 .at%), 63.58% (Hf14 .at%), 67.47% (Hf17 .at%) and 65.08% (Hf20 .at%). Close values confirm the uniform homogeneity of the 5 compositions, besides expressing a good level of crystallization during processing.

As an example, Figure 3 presents in detail the form by which X_c (%) was calculated in the alloy with 11 .at% of hafnium.

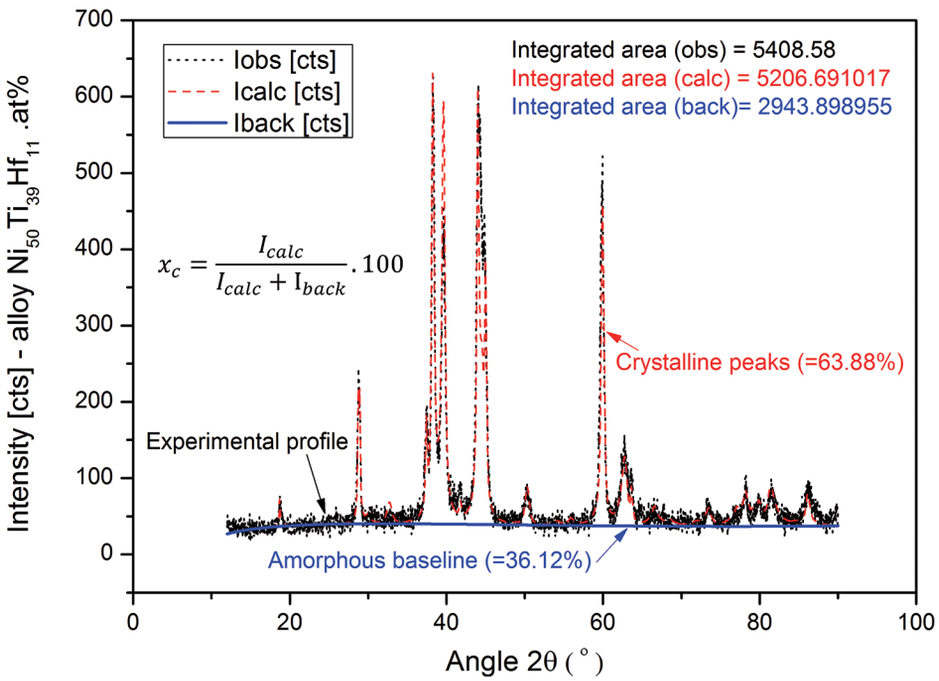

Figure 3
Visual separation of the 3 Intensities: observed (experimental), calculated and background.

In relation to minority phases, nucleation of the R phase at Ni-Ti alloys has been associated with the precipitated phase Ni_4Ti_3 (Khalil-Allafi *et al.*, 2002a; Khalil-Allafi *et al.*, 2002b; Wu *et al.*, 2010). It has also been observed by (Wu *et al.*, 2010) that precipitation of Ti_2Ni may also induce formation of the R phase. Herein, formation of the R phase is related to precipitation of the $(Ti, Hf)_2$ Ni phase (Yi *et al.*, 2017). Figure 2 presents X-ray diffraction patterns showing the coexistence of the R and $(Ti, Hf)_2$ Ni phases. Hence, precipitation of $(Ti, Hf)_2Ni$ may play an important role in the sequence of transformation in Ni-Ti-Hf alloys. According to literature (Suresh *et al.*,

2014), an increase in the amount of Hf in the alloy favors a decrease in the amount of (Ti, Hf)$_2$ Ni phase, as shown in Figure 4. This precipitation at the grain boundary creates a coherent/semi-coherent interface between the precipitate (Ti, Hf)$_2$ Ni and the matrix, which may intensify the driving force for formation of the R phase. According to Figure 4, considering the relative crystallinity (X_c) of each composition, an increase in the amount of the R phase was experimentally observed and is related with the addition of Hf and Ni (Karaca *et al.*, 2011).

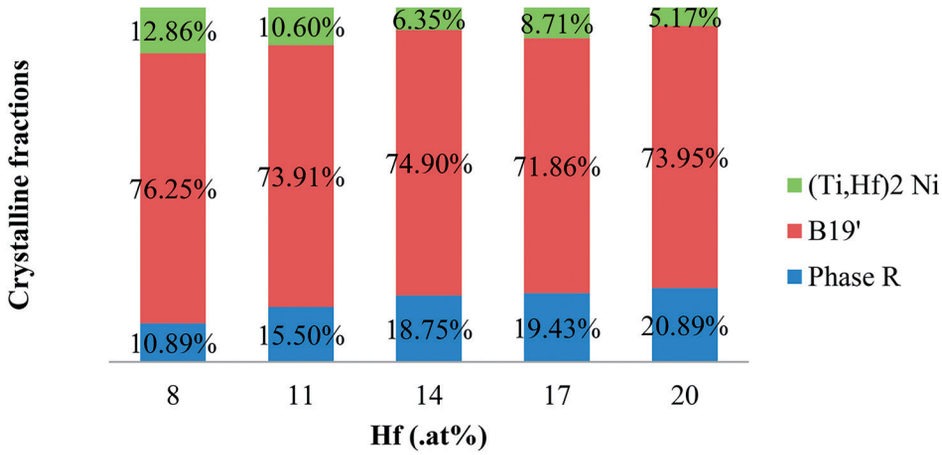

Figure 4
Crystalline fractions of the three identified phases.

Figure 5 presents DSC thermograms of studied alloys. The sorting by composition shows that TT are directly proportional to the gradual addition of Hf, replacing Ti.

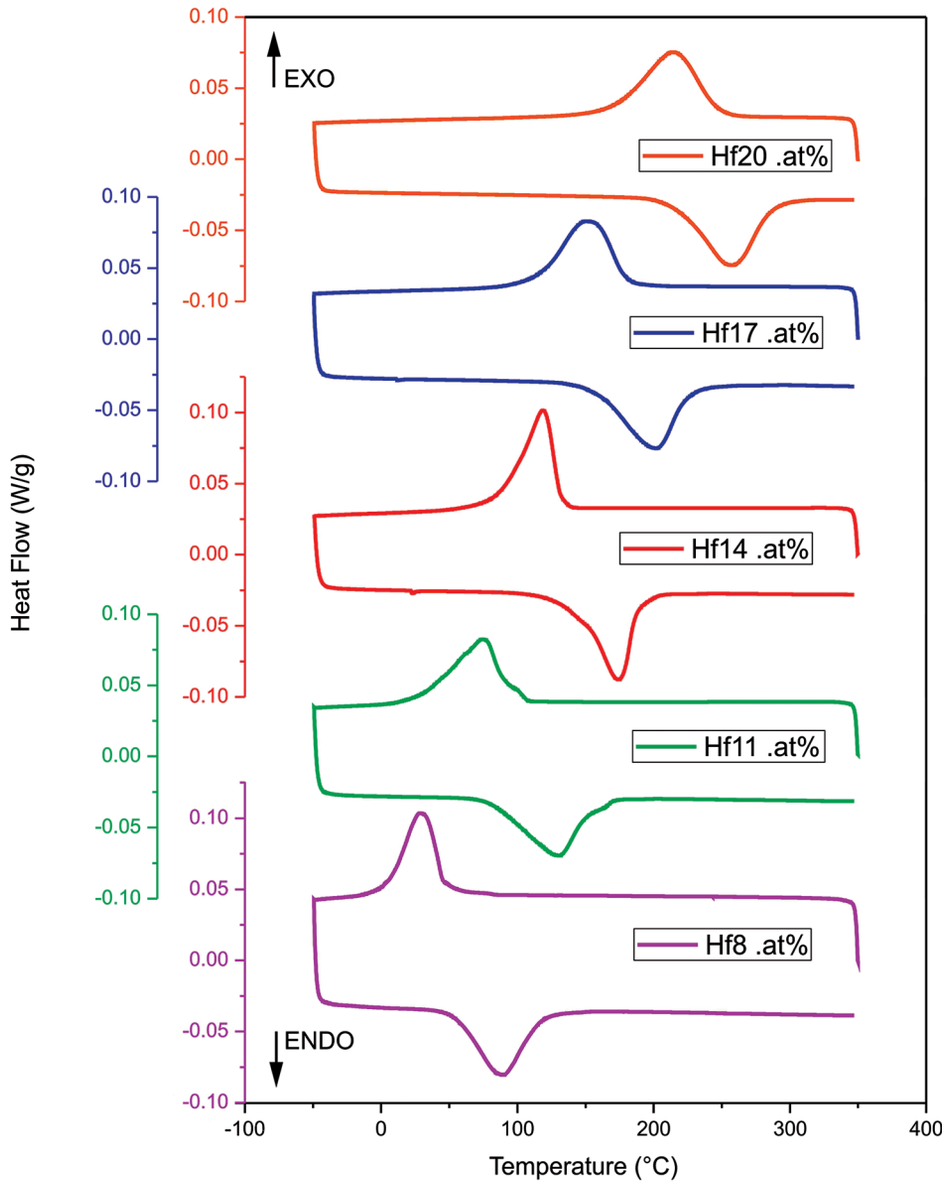

Figure 5
DSC results for the 5 nominal compositions of $Ni_{50}Ti_{50-X}Hf_X$ .at% alloys.

Despite the DSC, the thermograms present just one transformation peak at heating and cooling, low values of total hysteresis (ΔT = Af − Ms) and the diffractograms indicate a two-step transformation of the Ni-Ti-Hf alloys, which are: B2 → R → B19' (Suresh *et al.*, 2014).

Considering the martensitic matrix (R + B19'), according to Figure 6, percentage values of both instable phases are inversely proportional and establish logarithmic relationships. Decreasing values of total hysteresis establish a linear function and indicate that the R phase (rhombohedral) is more unstable than B19' (monoclinic).

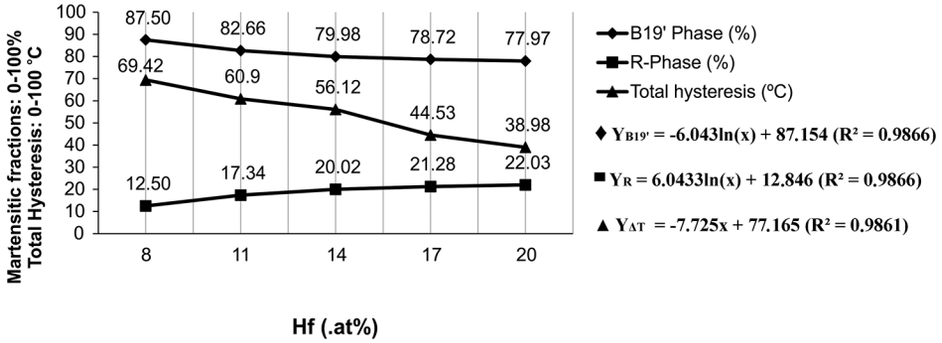

Figure 6
Martensitic portion (R + B19') and its relationship with total hysteresis (ΔT).

The presence of precipitates inhibits the transformation B2 → B19' while favoring the transformation B2 → R (Moshref-Javadi *et al.*, 2013). As Hf is added, the alloys get richer in nickel and consequently reduce the formation of precipitates at grain boundaries, as shown by diffractometry results. Hence, it is possible to conclude that in Ni-Ti-Hf-based alloys, the transformation B2 → R is more affected by the amount of nickel than by the effect of precipitates (Moshref-Javadi *et al.*, 2013).

Transformation temperatures are summarized in Table 4. The increase of TT in HSTMA alloys of Ni-Ti systems are probably also related to the fact that the third element atomic radius and melting point are higher than Ni's and Ti's. In our case, it is observed once the hafnium atomic radius is 1.55 Å and its melting point is 2232.85 °C, while nickel has r = 1.24 Å and T_m = 1454.85 °C, the same way Ti presents r = 1.40 Å and T_m = 1667.85 °C (Lide, 1999). Furthermore, some authors (Potapov *et al.*, 1997; Firstov *et al.*, 2004; Evirgen *et al.*, 2015) attribute the increase of transformation temperature in Ni-Ti-Hf to the increase in volume of the unit cell on martensitic transformation B19', which increases the stored elastic energy.

Compositions	Transformation Temperatures (°C)				Af − Ms (°C)	Enthalpies (J/g)	
Hf_X .at%	Ms	Mf	As	Af	Total Hysteresis	Ms → Mf	As → Af
Hf_8 .at%	45.58	5.77	55.30	115.00	69.42	10.36	10.75
Hf_{11} .at%	93.55	31.08	80.30	154.45	60.90	11.63	11.40
Hf_{14} .at%	131.98	90.35	145.32	188.10	56.12	11.85	12.21
Hf_{17} .at%	179.78	115.68	157.29	224.31	44.53	12.76	12.38
Hf_{20} .at%	247.17	171.54	216.46	286.15	38.98	13.41	13.18

Table 4
Transformation Temperatures (TTs) measured for $Ni_{50}Ti_{50-X}Hf_X$ .at% alloys.

Total enthalpies (μ = 12 J/g), shown in the last column of Table 2, have close values which indicates energy densities consistent with those that are normally required in the shear of atomic blocks of the crystalline network (>10 J/g).

It can be seen in the SEM micrograph of Figure 7 that the microstructure consists of precipitates of the $(Ti,Hf)_2$ Ni phase formed preferentially at grain boundaries of the Ni-Ti-Hf matrix. Grain boundaries act like preferential nucleation sites for the precipitated phase because they minimize the interfacial energy between matrix and precipitates.

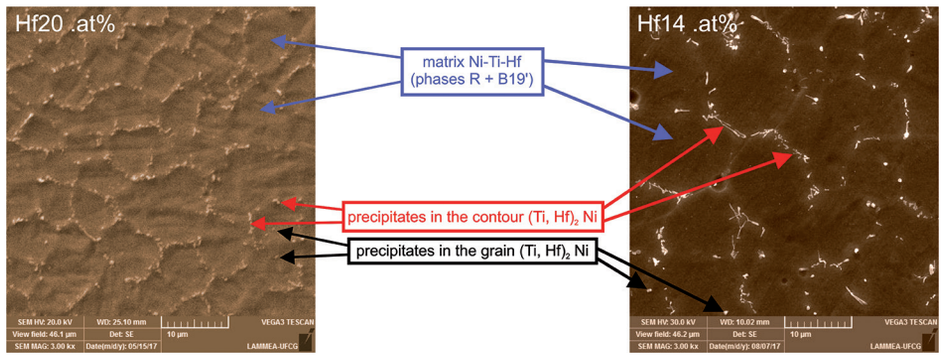

Figure 7
Identification of matrix phase (R + B19') and precipitated phase $(Ti, Hf)_2$ Ni.

Heterogeneous lenticular precipitation of the $(Ti, Hf)_2$ Ni phase occurs due to its nucleation being preferentially at grain boundaries. While diffusivity at the grain boundary is larger than the diffusivity at crystalline network, precipitation at the grain boundary is expected. Because of the concentration gradient at grain boundaries, resultant of the solute rejection during

formation of $(Ti, Hf)_2$ Ni phase, solute atoms diffuse through the crystalline network toward the grain boundaries. Coherent or semi-coherent planar interfaces are formed when interface energy between matrix and precipitate is minimum. Therefore, the occurrence of these interfaces is strongly dependent of the orientation of grain boundaries. However, the presence of planar interfaces may intensify a driving force to promote the transformation of the R phase in the alloy (Suresh *et al.*, 2014).

Reduction of transformation hysteresis due to redistribution of Ni, has been reported in literature (Meng *et al.*, 2001). However, for the alloys of the present study, a compositional change does not seem to be the only reason for low values of hysteresis observed in Table 4. Enrichment of the alloys by Ni have a greater effect on Ms temperature than on As or Af temperatures (Meng *et al.*, 2002), as shown in table 4.

The $(Ti, Hf)_2$ Ni precipitate is richer in Ti compared to Hf. However, the amount of Hf in $(Ti, Hf)_2$ Ni phase, present in the matrix, is always higher than the amount of Ti, according to Figures 8(a) and 8(b). Thus, considering only the precipitated phase $(Ti, Hf)_2$ Ni, the higher amount of Hf in the matrix compensates the Ti loss. The atomic quantification of these elements is organized in the first two lines of Table 5.

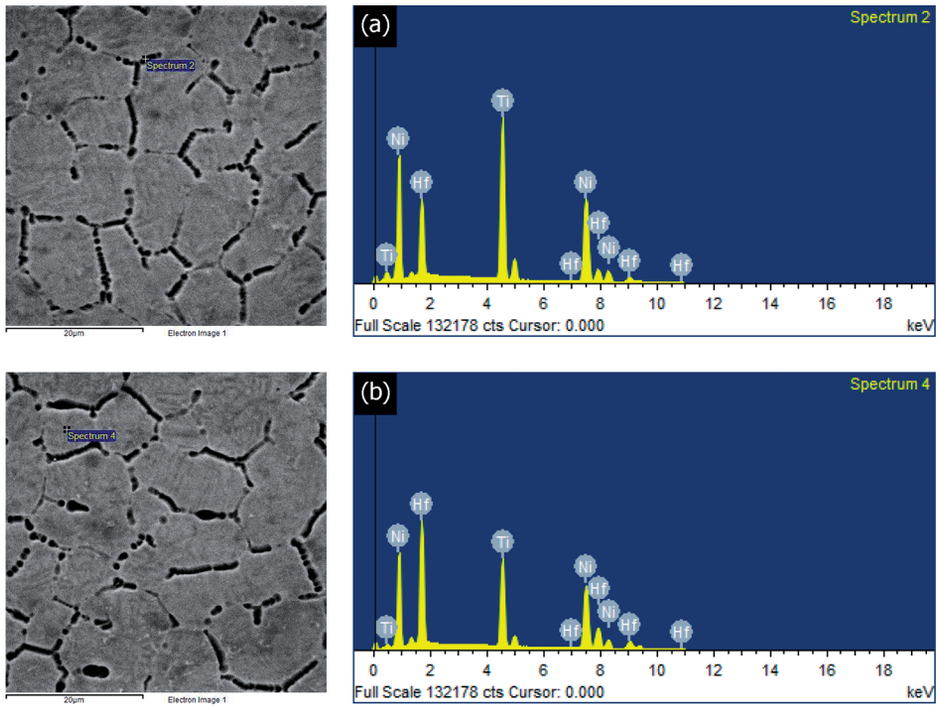

Figure 8
Punctual measurements of $(Ti, Hf)_2$ Ni phase present at grain boundary (spectrum 2) and inside the grain (spectrum 4).

In relation to the martensitic matrix Ni-Ti-Hf phase, the amount of the elements were quantified by EDS. Results are shown in Table 5 and are close to the values adopted as nominal. This reinforces the idea that the preparation of the alloys had an acceptable level of precision due to the proximity of the values measured by EDS to the theoretical values.

Table 5
Quantification of elements contained in the precipitate and martensite phases (by EDS – semi-quantitative results).

Position	Compound	Ni .at%	Ti .at%	Hf .at%
Contour	$(Ti, Hf)_2$ Ni	31.45	38.79	29.76
Matrix (grain)	$(Ti, Hf)_2$ Ni	34.28	23.45	44.17
Matrix (grain)	$Ni_{50}Ti_{42}Hf_8$ .at%	48.30	44.38	7.32
	$Ni_{50}Ti_{39}Hf_{11}$ .at%	49.55	39.9	10.55
	$Ni_{50}Ti_{36}Hf_{14}$ .at%	50.02	36.94	13.04
	$Ni_{50}Ti_{33}Hf_{17}$ .at%	49.89	33.85	16.26
	$Ni_{50}Ti_{30}Hf_{20}$ .at%	49.58	32.13	18.29

4. Conclusions

The influence of the amount of Hf on transformation temperatures and on microstructural evolution of $Ni_{50}Ti_{50-X}Hf_X$ .at% shape-memory alloys was studied. Based on experimental results, correlated with literature, it may be concluded that:

1. The microstructure consists of $(Ti, Hf)_2$ Ni precipitates formed preferentially at the grain boundaries of the Ni-Ti-Hf (R + B19') phase;

2. The increase in the amount of Hf in the alloy favors reduction in the amount of $(Ti, Hf)_2$ Ni phase, which precipitates at grain boundaries;

3. The $(Ti, Hf)_2$ Ni phase forms a coherent/semi-coherent interface between the $(Ti, Hf)_2$ Ni precipitate and the matrix, which may intensify the driving force to formation of the R phase;

4.The increase in the amount of Hf in Ni-Ti-Hf alloys increases phase transformation temperatures as well as the volume of monoclinic structures (B19' phase), but also favors the reduction of total hysteresis.

Acknowledgments

The authors would like to thank the CNPq for the financial support.

References

BESSEGHINI, S., VILLA, E., TUISSI, A. Ni-Ti-Hf shape memory alloy: effect of aging and thermal cycling. ***Materials Science and Engineering: A,*** v. 273-275, p. 390-394, 1999. ISSN 0921-5093. [https://doi.org/10.1016/S0921-5093(99)00304-4]

COLMAN, T. A. D., DEMIATE, I. M., SCHNITZLER, E. The effect of microwave radiation on some thermal, rheological and structural properties of cassava starch. ***Journal of Thermal Analysis and Calorimetry,*** v. 115, n. 3, p. 2245-2252, March 01 2014. ISSN 1588-2926. [https://doi.org/10.1007/s10973-012-2866-5]

EVIRGEN, A., KARAMAN, I., SANTAMARTA, R., PONS, J., NOEBE, R. D. Microstructural characterization and shape memory characteristics of the Ni50.3Ti34.7Hf15 shape memory alloy. ***Acta Materialia,*** v. 83, p. 48-60, 2015. ISSN 1359-6454. [https://doi.org/10.1016/j.actamat.2014.09.027]

FIRSTOV, G., VAN HUMBEECK, J., KOVAL, Y. N. Comparison of high temperature shape memory behaviour for ZrCu-based, Ti–Ni–Zr and Ti–Ni–Hf alloys. ***Scripta Materialia,*** v. 50, n. 2, p. 243-248, 2004. ISSN 1359-6462. [https://doi.org/10.1016/j.scriptamat.2003.09.010]

GONG, C., WANG, Y., YANG, D. Phase transformation and second phases in ternary Ni–Ti–Ta shape memory alloys. ***Materials chemistry and physics,*** v. 96, n. 2, p. 183-187, 2006. ISSN 0254-0584. [https://doi.org/10.1016/j.matchemphys.2005.06.057]

HUMBEECK, J. V. Shape memory alloys with high transformation temperatures. ***Materials Research Bulletin,*** v. 47, n. 10, p. 2966-2968, 2012. ISSN 0025-5408. [https://doi.org/10.1016/j.materresbull.2012.04.118]

KARACA, H. E., SAGHAIAN, S. M., BASARAN, B., BIGELOW, G. S., NOEBE, R. D., CHUMLYAKOV, Y. I. Compressive response of nickel-rich NiTiHf high-temperature shape memory single crystals along the [1 1 1] orientation. ***Scripta Materialia,*** v. 65, n. 7, p. 577-580, 2011. ISSN 1359-6462. [https://doi.org/10.1016/j.scriptamat.2011.06.027]

KARACA, H. E., SAGHAIAN, S. M., DED, G., TOBE, H., BASARAN, B., MAIER, H. J., NOEBE, R. D., CHUMLYAKOV, Y. I. Effects of nanoprecipitation on the shape memory and material properties of an Ni-rich NiTiHf high temperature shape memory alloy. ***Acta Materialia,*** v. 61, n. 19, p. 7422-7431, 2013. ISSN 1359-6454. [https://doi.org/10.1016/j.actamat.2013.08.048]

KHALIL ALLAFI, J., REN, X., EGGELER, G. The mechanism of multistage martensitic transformations in aged Ni-rich NiTi shape memory alloys. ***Acta Materialia,*** v. 50, n. 4, p. 793-803, 2002. ISSN 1359-6454. [https://doi.org/10.1016/S1359-6454(01)00385-8]

KHALIL-ALLAFI, J., DLOUHY, A., EGGELER, G. Ni4Ti3-precipitation during aging of NiTi shape memory alloys and its influence on martensitic phase transformations. ***Acta Materialia,*** v. 50, n. 17, p. 4255-4274, 2002. ISSN 1359-6454. [https://doi.org/10.1016/S1359-6454(02)00257-4]

KOCKAR, B., ATLI, K. C., MA, J., HAOUAOUI, M., KARAMAN, I., NAGASAKO, M., KAINUMA, R. Role of severe plastic deformation on the cyclic reversibility of a Ti50.3Ni33.7Pd16 high temperature shape memory alloy. ***Acta materialia,*** v. 58, n. 19, p. 6411-6420, 2010. ISSN 1359-6454. [https://doi.org/10.1016/j.actamat.2010.08.003]

KOVARIK, L., YANG, F., GARG, A., DIERCKS, D., KAUFMAN, M., NOEBE, R. D., MILLS, M. J. Structural analysis of a new precipitate phase in high-temperature TiNiPt shape memory alloys. ***Acta materialia,*** v. 58, n. 14, p. 4660-4673, 2010. ISSN 1359-6454. [https://doi.org/10.1016/j.actamat.2010.04.039]

LIDE, David R. Editor-in-Chief. CRC Handbook of Chemistry and Physics. 1999-2000. CRC press. 1999. (ISBN-10: 0849304806)

MA, J., KARAMAN, I., NOEBE, R. D. High temperature shape memory alloys. ***International Materials Reviews,*** v. 55, n. 5, p. 257-315, 2010. ISSN 0950-6608. [https://doi.org/10.1179/095066010X12646898728363]

MANCA, A., SHELYAKOV, A. V., AIROLDI, G. Ageing in parent phase and Martensite stabilization in a Ni50Ti30Hf20 alloy. ***Materials Transactions,*** v. 44, n. 6, p. 1219-1224, 2003. ISSN 1345-9678. [DOI: 10.2320/matertrans.44.1219]

MENG, X. L., CAI, W., WANG, L. M., ZHENG, Y. F., ZHAO, L. C., ZHOU, L. M. Microstructure of stress-induced martensite in a Ti–Ni–Hf high temperature shape memory alloy. ***Scripta Materialia,*** v. 45, n. 10, p. 1177-1182, 2001. ISSN 1359-6462. [https://doi.org/10.1016/S1359-6462(01)01147-2]

MENG, X. L., CAI, W., ZHENG, Y. F., TONG, Y. X., ZHAO, L. C., ZHOU, L. M. Stress-induced martensitic transformation behavior of a Ti–Ni–Hf high temperature shape memory alloy. ***Materials Letters,*** v. 55, n. 1, p. 111-115, 2002. ISSN 0167-577X. [https://doi.org/10.1016/S0167-577X(01)00631-0]

MOSHREF-JAVADI, M., HOSSEINSEYEDEIN, S., TAGHISALEHI, M., ABOUTALEBI, M. R. Age-induced multi-stage transformation in a Ni-rich NiTiHf alloy. ***Acta Materialia,*** v. 61, n. 7, p. 2583-2594, 2013. ISSN 1359-6454. [https://doi.org/10.1016/j.actamat.2013.01.037]

POTAPOV, P. L., SHELYAKOV, A. V., GULYAEV, A. A., SVISTUNOV, E. L., MATVEEVA, N. M., HODGSONC, D. Effect of Hf on the structure of Ni-Ti martensitic alloys. ***Materials Letters,*** v. 32, n. 4, p. 247-250, 1997. ISSN 0167-577X. [https://doi.org/10.1016/S0167-577X(97)00037-2]

RIETVELD, H. Line profiles of neutron powder-diffraction peaks for structure refinement. ***Acta Crystallographica,*** v. 22, n. 1, p. 151-152, 1967. ISSN 0365-110X. [https://doi.org/10.1107/S0365110X67000234]

RIETVELD, H. A profile refinement method for nuclear and magnetic structures. ***Journal of applied Crystallography,*** v. 2, n. 2, p. 65-71, 1969. ISSN 1600-5767. [https://doi.org/10.1107/S0021889869006558]

SANJABI, S., CAO, Y. Z., BARBER, Z. H. Multi-target sputter deposition of Ni-50Ti50–XHfX shape memory thin films for high temperature microactuator application. ***Sensors and Actuators A: Physical,*** v. 121, n. 2, p. 543-548, 2005. ISSN 0924-4247. [https://doi.org/10.1016/j.sna.2005.04.006]

SHI, H., DELVILLE, R., SRIVASTAVA, V., JAMES, R. D., SCHRYVERS, D. Microstructural dependence on middle eigenvalue in Ti–Ni–Au. ***Journal of Alloys and Compounds,*** v. 582, p. 703-707, 2014. ISSN 0925-8388. [DOI: 10.1016/j.jallcom.2013.08.132]

SOARES, R., CASTRO, W. B., SIMÕES, J. B.. Use of the Roniere´s Method in the preparation of smart alloy Ni-Ti-Hf. Proceedings of II World Congress on Computer Science, Engineering and Technology Education. September 04-07, 2016. In: ROCHA BRITO, C. da, (ISBN 978-85-65992-59-6), CIAMPI, M. M. In: (ISBN 978-85-66680-59-1). (Org.). Science and Education Research Council, COPEC - Castelo Branco, Portugal. p. 85-89. [DOI: 10.14684/WCCSETE.2.2016.85-89]

SONNEVELD, E., VISSER, J. Automatic collection of powder data from photographs. ***Journal of Applied Crystallography,*** v. 8, n. 1, p. 1-7, 1975. ISSN 1600-5767. [https://doi.org/10.1107/S0021889875009417]

SURESH, K. S., KIM, D-I., BHAUMIK, S. K., SUWAS, S. Evolution and stability of phases in a high temperature shape memory alloy $Ni_{49}.4Ti_{38}.6Hf_{12}$. ***Intermetallics,*** v. 44, p. 18-25, 2014. ISSN 0966-9795. [https://doi.org/10.1016/j.intermet.2013.08.005]

WU, L.-M., CHANG, S.-H., WU, S.-K. Precipitate-induced R-phase in martensitic transformation of as-spun and annealed $Ti_{51}Ni_{49}$ ribbons. ***Journal of Alloys and Compounds,*** v. 505, n. 1, p. 76-80, 2010. ISSN 0925-8388. [https://doi.org/10.1016/j.jallcom.2010.06.019]

YI, X., SUN, K. GAO, W., MENG, X., CAI, W., ZHAO, L. Microstructure design of the excellent shape recovery properties in $(Ti,Hf)_2Ni$/Ti-Ni-Hf high temperature shape memory alloy composite. ***Journal of Alloys and Compounds,*** v. 729, p. 758-763, 2017. ISSN 0925-8388. [https://doi.org/10.1016/j.jallcom.2017.09.242]

ZARINEJAD, M., LIU, Y., WHITE, T. J. The crystal chemistry of martensite in NiTiHf shape memory alloys. ***Intermetallics,*** v. 16, n. 7, p. 876-883, 2008. ISSN 0966-9795. [https://doi.org/10.1016/j.intermet.2008.04.004]

Received: 22 May 2018 - Accepted: 21 November 2018.